L_0 NORM OPTIMIZATION IN SAR IMAGE RECONSTRUCTION BASED ON SPARSE DECOMPOSITION

Prof. DrSc. Andon Lazarov
Assist. Prof. Dimitar Minchev, PhD
Burgas Free University

***Abstract**: Synthetic Aperture Radar SAR) image reconstruction algorithms based sparse decomposition is considered. The linear frequency modulated (LFM) signal reflected from the scene, relief of the Earth surface is presented as matrix multiplication of three matrices: azimuth Inverse Discrete Fourier Transform (IDFT) matrix, image matrix and range IDFT matrix. L0 norm optimization image reconstruction procedure is applied over reduced number of measurements defined by randomly generated azimuth and range sensing matrix. The geometry of the scene is described by standard Matlab „peaks" function. Results of numerical experiments are provided.*

***Key words**: SAR, Compressed Sensing*, l_0 norm optimization, Sparse Decomposition.

1. Introduction

The ability of Synthetic aperture radar (SAR) to obtain images of illuminated objects with high resolution independent of weather circumstances makes it preferable tool for surveillance, topographic mapping, flight navigation and target recognition. SAR has many remote sensing applications in military and civilian areas. In case of conventional SAR imaging algorithms, the high resolution of range direction is obtained by the pulse compression of Linier Frequency Modulated (LFM) signal, and the high resolution of azimuth direction is achieved through the aperture synthesis performed by the platform movement [1]. While SAR imaging theoretical limitation in sampling rate is defined by Shannon's theorem. It means the sampling rate must be at least twice the maximum frequency of the echo signal (the so-call Nyquist rate) [2]. Thus, algorithms for SAR imaging such as Range-Doppler algorithm [4], Chirp-Scaling algorithm [5], Spectral Analysis algorithm [6], based on correlation and matched filtering approaches can be applied. These algorithms may include Fourier transforms and different time-frequency transforms and are distinguished with different obstacles. The range resolution is limited by the bandwidth of transmitted signal, whereas the azimuth resolution is proportional to the synthetic aperture length which is limited by the kinematic parameters of the radar system, therefore high resolution SAR imaging is difficult to be achieved with low bandwidth and short aperture. The increasing number of samples to achieve high range resolution leads to computation burden. In addition, the correlation nature of the Fourier transforms used for SAR imaging yields high level sidelobes and interference problems.

To avoid aforementioned drawbacks a new computational technique named compressed sensing (CS) is created for signal and image reconstruction [7, 8]. CS allows certain signals and images to be recovered with far fewer samples or measurements than correlation and spectral methods require. Necessary condition to apply CS recovery procedure is the signal to be sparse or compressible in time, space and frequency domains. Thus, through application of CS, different efficient schemes have been created for signal and image reconstruction that requires much smaller sampling rate than the sampling rate Nyquist theorem requires. Based on its compressed sampling and exact reconstruction

ability, CS has been widely applied in different application areas, for example, data acquisition, communications, remote sensing, computational biology, medicine imaging, radar, etc. [9, 11].

It is worth noting some applications in radar signal processing field. A compressive sensing data acquisition and imaging system for Ground Penetrating Radar (GPR) is proposed in [12, 13], where instead of sampling radar echo at Nyquist rate, linear projections of return signals with some random vectors are used as measurements. A similar approach for through-wall radar imaging is discussed in [14]. A method to reduce the amount of stored SAR raw data based on CS is proposed in [15]. A radar imaging algorithm based on CS is presented in [16] and [17]. Resolution enhancement in ISAR imaging in case of low SNR via CS is described in [18]. Compressive sensing in the context of electromagnetic modeling of multi-static scattering from an arbitrary target is discussed in [19]. Imaging of sparse targets reconstructed by solving a convex optimization problem based on l_1 norm minimization with only a small number of SAR echo samples is described in [20]. All results show that the CS method outperforms the conventional correlation methods, even if very small random selected samples are used. A method for range focusing by a pulse compression technique, which improves SNR level in both azimuth and cross-track directions, and enhances images of sparse targets reconstructed by l_1 norm regularization is presented in [21].

In conclusion, CS approach can be applied in many SAR applications such as monitoring of a mountain area with prominent peaks, ships on a sea surface and city area with dominant point-like-targets distributed in a sparse way over illuminated scene. It is only required the number of dominant scatterers to be much smaller than the number of overall samples of illuminated scene. It means that SAR return can be considered as a sparse signal.

To overcome the resolution limitation of conventional SAR imaging algorithms defined by Nyquist sampling theorem, in the present paper a SAR imaging algorithm based on compressed sensing and l_0 norm optimization in case of sparse image decomposition is discussed. The advantage of the suggested CS method is that a higher resolution image is obtained based on fewer measured data than measurements required by sampling Nyquist constrains. The main strong scatterers intensities are extracted by constructing a time-frequency overcomplete Fourier dictionary. Numerical simulations are carried out to evaluate the correctness of the suggested method. The results show that the developed CS method outperforms the conventional spectral correlation imaging algorithms in number of measurements, robustness and resolution capabilities.

2. SAR geometry

Consider SAR geometry and kinematic scenario, defined in coordinate system *Oxyz*. SAR system is located on a spacecraft platform with pre-defined trajectory parameters. The spacecraft's movement is given by the following vector equation

$$\mathbf{R}(p) = \mathbf{R}_0 + \mathbf{V}T_p\left(\frac{N}{2} - p\right), \tag{1}$$

where $\mathbf{R}_0 = \mathbf{R}(0)$ is the distance vector from the origin of the coordinate system to the satellite in the moment $t = 0$; $\mathbf{V}$ is the satellite velocity vector; T_p is the signal repetition period ; p is the index of emitted pulses; N – is the full number of emitted pulses.

The projection of the vector equation (1) on the coordinate system *Oxyz* yields

$$\begin{aligned} x(p) &= x_0 - V_x T_p \left(\frac{N}{2} - p \right) \\ y(p) &= y_0 - V_y T_p \left(\frac{N}{2} - p \right), \\ z(p) &= z_0 - V_z T_p \left(\frac{N}{2} - p \right) \end{aligned} \tag{2}$$

where $x(p)$, $y(p)$ and $z(p)$ are the satellite coordinates in the moment p; $x_0 = x(0)$, $y_0 = y(0)$ and $z_0 = z(0)$ are the satellite coordinates in the moment $p = 0$; $V_x = V\cos\alpha$, $V_y = V\cos\beta$, $V_z = V\cos\delta$ are coordinates of the velocity vector; $\cos\alpha$, $\cos\beta$, $\cos\gamma$ are the guiding cosines of the velocity vector.

The surface under observation is depicted in coordinate system *Oxyz* and analytically can be presented as a function of surface, i.e. *z* as a function of coordinates *x* and *y*, which in discrete form is described by the following equation

$$\begin{aligned} z_{mn} &= z_{mn}(x_{mn}, y_{mn}) = 3(1 - x_{mn})^2 \exp\left[-(x_{mn})^2 - (y_{mn} + 1)^2 \right] \\ &- 10\left(\frac{x_{mn}}{5} - x_{mn}^{\,3} - y_{mn}^{\,5} \right) \exp\left[x_{mn}^{\,2} - y_{mn}^{\,2} \right] \\ &- \frac{1}{3} \exp\left[-(x_{mn} + 1)^2 - y_{mn}^{\,2} \right] \end{aligned} \tag{3}$$

where $x_{mn} = m\Delta M$ and $y_{mn} = n\Delta N$ are discrete coordinates in the plane *Oxy*; ΔM and ΔN are dimensions of the resolution element in the plane *Oxy*; m and n – relative discrete coordinates (coordinate indexes of the resolution element) on axes *Ox* and *Oy*. Coordinates x_{mn}, y_{mn} and z_{mn} define distance vector $\mathbf{R}_{mn}$ of each point scatterer.

Assume in each resolution element with dimensions (ΔM, ΔN) and coordinates (x_{mn}, y_{mn}) one prominent point scatterer is located. During the process of observation the distance vector $\mathbf{R}_{mn}(p)$ from SAR located on the satellite to the dominant point scatterer, defined by the vector $\mathbf{R}_{mn}$, can be expressed by the following vector equation

$$\mathbf{R}_{mn}(p) = \mathbf{R}(p) - \mathbf{R}_{mn}\,. \tag{4}$$

The geometry of the observed surface can be extracted from the complex amplitude of the signal reflected from each point scatterer. The phase of the complex amplitude is proportional to the module of the distance vector $R_{mn}(p)$ defined by the expression

$$R_{mn}(p) = \sqrt{[x(p) - x_{mn}]^2 + [y(p) - y_{mn}]^2 + [z(p) - z_{mn}]^2}\,. \tag{5}$$

While modeling the process of observation the value of the parameter $R_{mn}(p)$ is calculated for each p, m and n. During program implementation the results of the calculation are placed into three dimensional matrix with discrete coordinates p, m, and n (Фиг. 1).

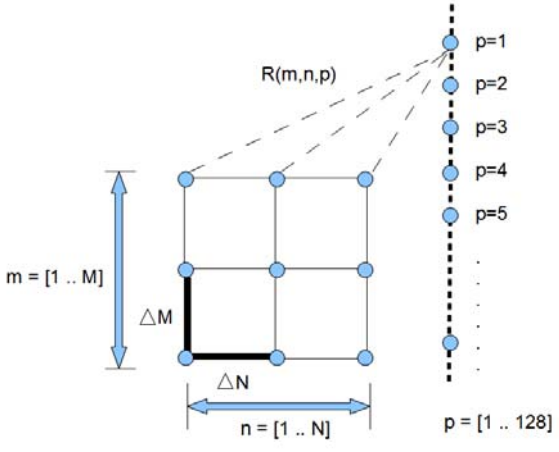

Fig.1. Three dimensional matrix of distances to prominent point scatterers on the observed surface

3. Modeling of SAR signal reflected from the observed surface

SAR illuminates the surface by series of LFM electromagnetic pulses, described by the equation

$$S(t) = \sum_{p=1}^{M} A \exp\left\{-j\left[\omega(t - pT_p) + b(t - pT_p)^2\right]\right\}, \quad (6)$$

where A is the amplitude of the emitted pulse, T_p is the pulse repetition period, $\omega = 2\pi\frac{c}{\lambda}$ is the angular frequency, $p = \overline{0,\ N-1}$ is the current number of emitted LFM pulse, N is the number of emitted pulses during aperture synthesis, c = 3.10^8 m/s is the speed of light, ΔF is the bandwidth of the emitted pulse, that defines the range resolution $\Delta R = c/2\Delta F$, $b = \frac{\pi\Delta F}{T_k}$ is the LFM rate, T_κ is the time duration of LFM pulse.

The deterministic component of the SAR signal reflected from the *mn*-th point scatterer is a finite function and can be written as

$$S_{mn}(t) = a_{mn}(z_{mn}).\mathbf{rect}\frac{t - t_{mn}}{T_k}.\exp\left\{-j\left[\omega(t - t_{mn}) + b(t - t_{mn})^2\right]\right\} \quad (7)$$

where

$$\mathbf{rect}\frac{t - t_{mn}(p)}{T_k} = \begin{cases} 0, if\ \frac{t - t_{mn}(p)}{T_k} \le 0 \\ 1, if\ 0 < \frac{t - t_{mn}(p)}{T_k} \le 1 \end{cases}, \quad (8)$$

is the rectangular function; $a_{mn}(z_{mn})$ is the reflectivity coefficient of the *mn*-th point scatterer from the surface of the observation, $t_{mn}(p)=\frac{2R_{mn}(p)}{c}$ is the time delay of the signal from the *mn*-th point scatterer.

The deterministic component of the SAR signal reflected from the entire surface can be regarded as a geometrical sum of signals reflected by all point scatterers from the surface of observation and can be expressed as

$$S(t)=\sum_{n}\sum_{m}a_{mn}(z_{mn}).\mathbf{rect}\frac{t-t_{mn}(p)}{T_k}.\exp\left\{-j\left[\omega\left(t-t_{mn}(p)\right)+b(t-t_{mn}(p))^2\right]\right\} \quad (9)$$

The fast time *t* measured in range direction for particular *p* and *k* in discrete form is written as

$$t=t_{mn\min}(p)+(k-1)\Delta T\,, \quad 10)$$

where $k=\overline{0,K_{\max}(p)-1}$ is the index of the range discrete, $\Delta T=1/2\Delta F$ is the time duration of the LFM sample, ΔF is the bandwidth of the emitted LFM pulse, $K_{\max}(p)$ is the number of the range bin where the SAR signal from the furthest point scatterer is detected, $t_{mn\min}(p)=\frac{2R_{mn\min}(p)}{c}$ is the time delay of the signal from the nearest point scatteter, $R_{mn\min}(p)$- is the distance to the nearest point scatteter on the surface of observation, defined for the *p*-th emitted pulse.

Taylor expansion of the term $\omega\left(t-t_{mn}(p)\right)+b(t-t_{mn}(p))^2$ in the vicinity of unknown discrete coordinates $\hat{p}$ and $\hat{k}$ corresponding to the *mn*-th point scatterer projected onto the image plane defined by the line of sight and SAR vector velocity, yields

$$\widetilde{S}(p,k)=\sum_{\hat{p},\hat{k}}a(\hat{p},\hat{k}).\mathbf{exp}\left\{-j\left[2.\pi.\frac{p.\hat{p}}{\hat{N}}+2.\pi.\frac{k.\hat{k}}{\hat{K}}+\Phi(p,k)\right]\right\}, \quad (11)$$

where $\Phi(p,k)$ is the higher order phase term, $\hat{p}=\overline{0,\hat{N}-1}$, $\hat{k}=\overline{0,\hat{K}-1}$, $\hat{N}$ and $\hat{K}$ denote the full number of reference image points on cross range and range directions, $a(\hat{p},\hat{k})$ is the 2-D image function. Assume $\Phi(p,k)=0$, then (11) in matrix form can be rewritten as [20]

$$\mathbf{S}=\mathbf{P}.\mathbf{A}.\mathbf{K}^T \quad (12)$$

where $\mathbf{S}(N\times K)$ is the measurement signal matrix, $\mathbf{P}(N\times\hat{N})=\left[\exp\left(-j\frac{2\pi p.\hat{p}}{\hat{N}}\right)\right]$ is the Discrete Fourier Transform (DFT) matrix (cross-range matrix-dictionary),

$\mathbf{K}(K \times \hat{K}) = \left[\exp\left(-j \frac{2\pi k.\hat{k}}{\hat{K}} \right) \right]$ is the DFT matrix (range matrix-dictionary), $\mathbf{A}(\hat{N} \times \hat{K})$ is the image matrix.

4. Sparse decomposition approach to solve the image reconstruction problem

Expression (12) denotes 2-D discrete Fourier decomposition of the signal in matrix form. It means that the two-dimensional signal $\mathbf{S} \in \mathbf{R}^{N \times K}$ is a linear combination of columns of matrices **P** and **K.** In case $N = \hat{N}$ (complete measurement) the decomposition (12) is unique, it means that there exists a unique sparsest solution for **A**. Define compressed (sensed) measurement matrix,

$$\mathbf{X} = \mathbf{\Phi}_p.\mathbf{S}.\mathbf{\Phi}_k^T + \mathbf{W} \in \mathbf{R}^{N' \times K'}, \tag{13}$$

over the redundant Fourier dictionaries $\hat{\mathbf{P}} = \mathbf{\Phi}_p.\mathbf{P} \in \mathbf{R}^{N' \times \hat{N}}$ and $\hat{\mathbf{K}} = \mathbf{\Phi}_k\mathbf{K}. = \mathbf{R}^{K' \times \hat{K}}$,

where $$\mathbf{\Phi}_p(N' \times N) \text{ and } \mathbf{\Phi}_k(K' \times K) \tag{14}$$

are pseudo identity sensing matrices**,** **W** is the white Gaussian noise matrix. In overcomplete case $N' < \hat{N}$ and $K' < \hat{K}$ the matrix **X** does not have unique decomposition. The image reconstruction problem can be solved by definition of sparse decomposition of the measurement signal

$$\mathbf{min}\|\mathbf{A}\|_0 \text{ subject to } \left\|\mathbf{X} - \hat{\mathbf{P}}.\mathbf{A}.\hat{\mathbf{K}}^T\right\|_2^2 \le \varepsilon, \tag{15}$$

where $\mathbf{min}\|\mathbf{A}\|_0$ is the l_0 – norm that denotes the number of non-zero point scatterer intensities in image matrix **A**. It means finding an image matrix **A** with as much zero entries as possible. The expression $\left\|\mathbf{X} - \hat{\mathbf{P}}.\mathbf{A}.\hat{\mathbf{K}}^T\right\|_2^2$ denotes the square of the Euclidian norm, ε is a small constant.

A Gaussian function is used to approximate the l_0 - norm, i.e.

5. Image reconstruction algorithm based on sparse decomposition

The modified image reconstruction algorithm:

1. Calculate initial estimate of the image matrix $\hat{\mathbf{A}}_0$, using Euclidian norm $\left\|\mathbf{X} - \hat{\mathbf{P}}.\mathbf{A}.\hat{\mathbf{K}}^T\right\|_2^2 = 0$, which corresponds to an initial variance $\sigma_0 = \infty$, i.e.

$$\hat{\mathbf{A}}_0 = \hat{\mathbf{P}}^*.\mathbf{X}.(\hat{\mathbf{K}}^*)^T, \tag{16}$$

where $\hat{\mathbf{P}}^* = \left[\exp\left(j \frac{2\pi p.\hat{p}}{\hat{N}} \right) \right]$, $\hat{\mathbf{K}}^* = \left[\exp\left(j \frac{2\pi k.\hat{k}}{\hat{K}} \right) \right]$ are the cross range and range inverse DFT matrices, respectively.

2. Define the next value of the variance $\sigma_1 = (2-4).(\max|\hat{a}_{\hat{p},\hat{k}}|)$ where $(\max|\hat{a}_{\hat{p},\hat{k}}|)$ is the maximum absolute value of an entry in the matrix $\hat{\mathbf{A}}_0$.

3. Define decreasing sequence of variances $\sigma_j = c.\sigma_{j-1}$, where $j = \overline{2,J}$, $0.5 \le c \le 1$, i.e. For each σ_{j-1}, calculate $F_\sigma(\hat{\mathbf{A}}) = \sum_{\hat{p}=0}^{\hat{N}-1}\sum_{\hat{k}=0}^{\hat{K}-1} \exp\left(-\frac{\hat{a}^2_{\hat{p},\hat{k}}}{2\sigma^2_{j-1}}\right)$ and $\left\|\hat{\mathbf{A}}\right\|_0$ using elements of $\hat{\mathbf{A}}_0$ (16).

Steepest ascending algorithm for SAR imaging

4. Initialization: Let $\mathbf{A} = \hat{\mathbf{A}}_{j-1}$, obtained for $\sigma = \sigma_{j-2}$.

Define the decreasing matrix $\mathbf{\Delta} = [\delta_{\hat{p},\hat{k}}] = [-\sigma^2_{j-2}.(\nabla F_{\sigma\, j-2})]$, where ∇ is the nabla operator over $F_{\sigma\, j-2}$, then $\delta_{\hat{p},\hat{k}} = \hat{a}_{\hat{p}.\hat{k}}.\exp\left(-\frac{\hat{a}^2_{\hat{p},\hat{k}}}{2\sigma^2_{j-2}}\right)$.

5. Calculate $\hat{\mathbf{A}}_j = \hat{\mathbf{A}}_{j-1} - \mathbf{\Delta}$. If $\hat{\mathbf{A}}_j < \hat{\mathbf{A}}_{j-1}$, go to step 3. In case the matrix $\hat{\mathbf{A}}_j$ does not change, then project matrix $\hat{\mathbf{A}}_{j-1}$ back onto the feasible set $\left\{\mathbf{A}\middle|\mathbf{X} = \hat{\mathbf{P}}.\mathbf{A}.\hat{\mathbf{K}}^T\right\}$, i.e.

$\mathbf{A}_j = \mathbf{A}_{j-1} - \hat{\mathbf{P}}^*(\hat{\mathbf{P}}.\mathbf{A}_{j-1}.\hat{\mathbf{K}}^T - \mathbf{X})(\hat{\mathbf{K}}^*)^T$.

6. The procedure is repeated until $\mathbf{A}_j = \mathbf{A}_{j-1}$ or $\|\mathbf{A}\|_0$ does not decrease anymore. In practice, the termination of the optimization procedure can be performed when $\left\|\mathbf{A}_{j-1}\right\|_0 - \left\|\mathbf{A}_j\right\|_0 \le 10^{-2}$.

6. Numerical experiment

Consider SAR scenario with the following parameters. Initial coordinates of the SAR carrier: $x_0 = 10^4$ m, $y_0 = 10^4$ m, $z_0 = 8.10^5$ m, vector velocity: $V = 10^3$ m, guiding angles: $\alpha = \pi \backslash 4$, $\beta = \pi \backslash 4$, $\gamma = 0$. SAR parameters: carrier frequency 10^{10} Hz, frequency bandwidth $2.5.10^7$ Hz, pulse repetition period $2.5.10^{-3}$, LFM pulse width $2.5.10^{-6}$, number of emitted pulses $N_p = 512$, number of range samples $K = 512$. Geometry of scene is defined by standard „peaks" Matlab function, displacement between point scatterers $\nabla M = \nabla N = 2$ m.

The full measurement signal complex matrix **S** (amplitude and phase) calculated by formula (9) is presented in Fig. 2,*a*. Compressed sensing measurement matrix **X** obtained by multiplication of the signal complex matrix **S** with sensing pseudo identity matrices (14) is presented in Fig. 2,*b*.

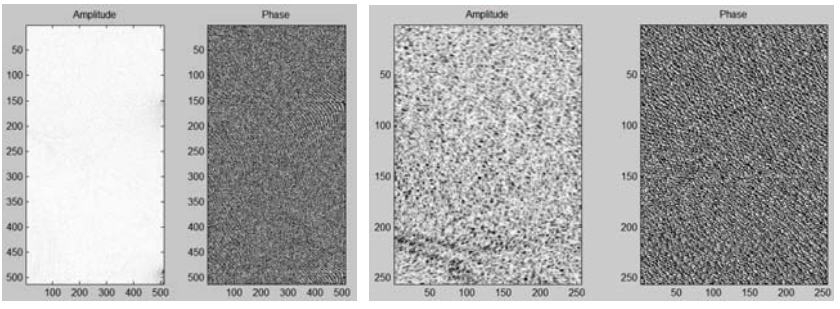

(a) *(b)*

*Fig. 2. Full measurement signal complex matrix **S** (amplitude and phase) (a) and compressed sensing **X** measurement matrix (b)*

Complex image matrix A_0 (amplitude (*a*) and phase (*b*)) obtained by formula (16) is presented in Fig. 3.

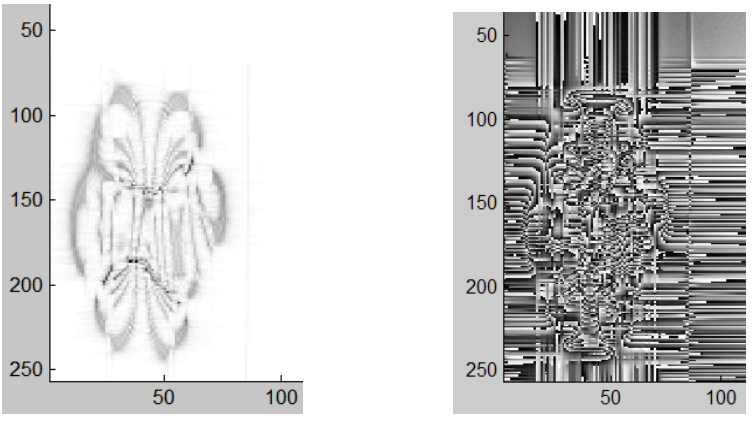

(a) *(b)*

Fig. 3. A_0 complex image (amplitude (a) and phase (b)) extracted by formula (14)

Final image obtained by application of the developed l_0 optimization image reconstruction algorithm based on sparse decomposition after 15 iterations is depicted in Fig. 4. As can be noticed the resolution of the final image is much better that the image A_0 in Fig. 3,*a*.

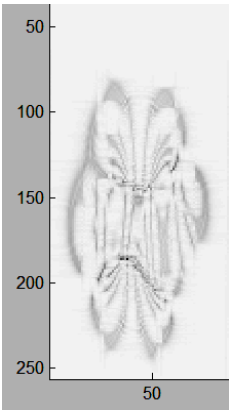

Fig. 4. Final image (amplitude) after 25 iterations

Conclusion

In the present paper SAR image reconstruction algorithms based on sparse decomposition of the image has been thoroughly discussed. The geometry of the scene is described analytically by standard function „peaks" in Matlab environment. The 2-D linear frequency modulated signal reflected from the scene, relief of the Earth surface has been presented as matrix multiplication of three matrices: azimuth Inverse Discrete Fourier Transform matrix, image matrix and range IDFT matrix. l_0 norm optimization image reconstruction procedure has been applied over reduced number of measurements defined by randomly generated azimuth and range sensing matrix. Results of numerical experiments have been provided in order to verify l_0 norm optimization algorithm.

Acknowledgment

This work is supported by project National Science Fund T02/3, 2014.

References:

1. Soumekh, M., *Synthetic Aperture Radar Signal Processing with Matlab Algorithms*, Wiley, New York, NY, 1999.
2. Curlander, J. C. and R. N. McDonough, *Synthetic Aperture Radar: Systems and Signal Processing*, John Wiley and Sons, 1991.
3. Cumming, I. G. and F. H. Wong, *Digital Processing of Syethetic Aperture Radar Data: Algorithm and Implementatoin*, Artech House Publishers, 2005.
4. Chan, Y. K. and V. C. Koo, „An introduction to synthetic aperture radar (SAR)", *Progress In Electromagnetics Research B*, Vol. 2, 27-60, 2008.
5. Moreira, A., J. Mittermayer, and R. Scheiber, „Extended chirp scaling algorithm for air- and spaceborne SAR data processing in stripmap and ScanSAR imaging modes", *IEEE Transactions on Geoscience and Remote Sensing*, Vol. 34, No. 5, 1123-1136, Sep. 1996.
6. Fang, L., X. Wang, and Y. Wang, „A modified SPECAN algorithm for synthetic aperture radar imaging", *International Conference on Measuring Technology and Mechatronics Automation*, Changsha, China, Mar. 2010.

7. Donoho, D., „Compressed sensing", *IEEE Trans. Inf. Theory*, Vol. 52, No. 4, pp. 289-1306, Apr. 2006.
8. Baraniuk, R., „Compressive sensing", *IEEE Signal Processing*, Vol. 24, No. 4, pp.118-121, Jul. 2007.
9. Candes, E. J. and M. Wakin, „An introduction to compressive sampling", *IEEE Signal Processing Magazine*, 21-30, Mar. 2008.
10. Romberg, J., „Imaging via compressive sampling", *IEEE Signal Processing*, Vol. 25, No. 2, 14-20, Mar. 2008.
11. Bruckstein, A. M., D. L. Donoho, and M. Elad, „From sparse solutions of systems of equations to sparse mofeling of signals and images", *SIAM Review*, Vol. 51, No. 1, pp. 34-81, Feb. 2009.
12. Gurbuz, A. C., J. H. McClellan, and W. R. Scott, Jr., „Compressive sensing for GPR imaging", *Proc. Asilomar Conf. Signals, Syst., Comput.*, pp. 2223-2227, Nov. 2007.
13. Gurbuz, A. C., J. H. McClellan, and W. R. Scott," A compressive sensing data acquisition and imaging method for stepped-frequency GPRs", *IEEE Transation on Signal Processing*, Vol. 57, No. 7, pp. 2640-2650, Jul. 2009.
14. Huang, Q., L. Qu, B. Wu, and G. Fang, „UWB Throug-wall imaging based on compressive sensing", *IEEE Transactions on Geoscience and Remote Sensing*, Vol. 48, No. 3, pp. 1408-1415, 2010.
15. Bhattacharya, S., T. Blumensath, B. Mulgrew, and M. Davies, „Fast encoding of synthetic aperture radar raw data using compressed sensing", *Proc. IEEE/SP Stat. Signal Process*, pp. 448-452, Madison, WI, Aug. 2007.
16. Baraniuk, R. and P. Steeghs, „Compressive radar imaging", *Proc.IEEE Radar Conf.*, pp. 128-133, Boston, MA, Apr. 2007.
17. Herman, M. A. and T. Strohmer, \High-resolution radar via compressed sensing, *„IEEE Transactions on Signal Processing*, Vol. 57, No. 6, pp. 275-2284, Jun. 2009.
18. Zhang, L., M. Xing, C. Qiu, et al., „Achieving higher resolution ISAR imaging with limited pulses via compressed sampling", *IEEE Geoscience and Remote Sensing Letters*, Vol. 6, No. 3, pp. 567-571, Jul. 2009.
19. Lawrence Carin, Dehong Liu, Wenbin Lin, Bin Guo. „Compressive sensing for multi-static scattering analysis", Journal of Computational Physics 228, pp. 3464–3477, 2009.
20. S.-J. Wei, X.-L. Zhang, J. Shi, and G. Xiang. „Parse reconstruction for SAR imaging based on compressed sensing", Progress In Electromagnetics Research, Vol. 109, pp. 63-81, 2010.
21. S.-J. Wei, X.-L. Zhang, and J. Shi, „Linear array SAR imaging via compressed sensing" Progress In Electromagnetics Research, Vol. 117, 299-319, 2011.